Synthetic Strategies To Obtain V−P−O Open Frameworks Containing Organic Species as Structural Directing Agents. Crystal Structure of the V(IV)−Fe(III) Bimetallic Phosphate $[H_3N(CH_2)_2NH_3]_2[H_3N(CH_2)_2NH_2][Fe^{III}(H_2O)_2(V^{IV}O)_8(OH)_4(HPO_4)_4(PO_4)_4]\cdot 4H_2O$

Manuel Roca,[†] M. Dolores Marcos,[†] Pedro Amorós,*[,†] Aurelio Beltrán-Porter,[†] A. J. Edwards,[‡] and Daniel Beltrán-Porter[†]

UIBCM, Departament de Química Inorgánica, Facultat de Químiques, and Institut de Ciència dels Materials, Universitat de València, Dr. Moliner 50, 46100 Burjassot, València, Spain, and Department of Chemistry, University of Cambridge, Lensfield Road, Cambridge CB2 1EW, U.K.

Received February 28, 1996[⊗]

A general synthetic approach to rationalize the solution preparative chemistry of oxovanadium phosphates containing organic species as structural directing agents is presented. Careful attention is payed to the hydrolysis and condensation processes involving the ionic species in solution, and a simple restatement of the partial charge model (PCM) has been used in order to organize the experimental results. The structure of a new V(IV)−Fe(III) bimetallic oxovanadium phosphate, $[H_3N(CH_2)_2NH_3]_2[H_3N(CH_2)_2NH_2]$ $[Fe^{III}(H_2O)_2(V^{IV}O)_8(OH)_4(HPO_4)_4(PO_4)_4]\cdot 4H_2O$, has been determined by X-ray single crystal diffraction methods. This compound crystallizes in the monoclinic system, space group $P2_1/n$ and the cell dimensions are as follows: $a = 14.383(3)$ Å, $b = 10.150(2)$ Å, $c = 18.355(4)$ Å, and $\beta = 90.39(3)°$ ($Z = 2$). The existence of a complex intercrossing channel system, including a very large channel of 18.4 Å of diameter (in which both water molecules and ethylenediamine species are located), is the more interesting feature of this structure. Thermal decomposition, including the dehydration/rehydration process, has been studied by thermal analysis and variable temperature X-ray powder diffraction techniques. A complementary SEM study of the different intermediate decomposition products is presented.

Introduction

Microporous materials derived from tetrahedral frameworks currently boasts an extensive chemistry because a number of them display useful properties as catalysts, sorbents, and ionic exchangers.[1−4] In contrast, 3-D open "zeolitic" arrays are much less common in solids containing octahedrally coordinated d-block elements.[5] In this context, the interest on materials derived from the well-known catalytic V−P−O system[6,7] has recently received a new impulse because of the success of some synthesis tricks to get such open frameworks.[8]

A great number of A−V−P-O phases (A = organic or inorganic species) have been synthesized and characterized.[8,9] The variety of A species able to be incorporated to the basic array of phosphate tetrahedra and vanadyl octahedra is responsible for the dramatic expansion of the structural chemistry of these materials, including a diversity of lamellar and tunneled networks with the A species located in the structural voids. As a counterweight, when dealing with organic A species (frequently referred to as "templates" or "structural directing agents"), the complexity of the preparative chemistry outstandingly increases.

Hydrothermal synthesis in the presence of organic template species has becomed a convenient "soft chemistry" route to isolate new metastable microporous or open framework solids.[10] Notwithstanding, these procedures frequently lead to polyphasic products or suffer from problems such as poor yields or hardly reproducible results. As stated by Zubieta, "the ability to synthesize (this type of) solid materials according to rational designs is still somewhat primitive".[8] In practice, the lack of appropriate thermodynamic data and the "black-box" nature of the hydrothermal method are two of the main difficulties for predictions concerning both reaction mechanisms and products of synthesis. In fact, only a good knowledge of the solution chemistry of the precursor species in standard conditions might constitute an orientative reference in the search for rational designs through hydrothermal procedures.

Our synthesis strategy (which has proved its usefulness in dealing with transition metal oxophosphorous derivatives)[11] is based on a simple idea: the resulting framework in the final solid is affected by the nature of the ionic aggregates present in the mother solution. Thus, when one approaches the synthesis of transition metal containing oxoanionic derivatives, redox processes must be considered along with the hydrolytic ones and the subsequent condensation reactions.[12] In the present work we have used a modification of Livage's partial charge model (PCM) as an useful tool to organize the experimental results.[13] These are referred to the synthesis of one already known oxovanadium phosphate and a new material obtained

* Author to whom correspondence should be addressed.
[†] Universitat de València.
[‡] University of Cambridge.
[⊗] Abstract published in *Advance ACS Abstracts,* August 15, 1996.

(1) Wilson, S. T.; Lock, B. M.; Messina, C. A.; Cannan, T. R.; Flanigen, E. M. *J. Am. Chem. Soc.* **1982**, *104*, 1146.
(2) Szostak, R. *Molecular Sieves: Principle of Synthesis and Identification*; Van Nostrand Reinhold: New York, 1989.
(3) Barrer, R. M. *Hydrothermal Chemistry of Zeolites*; Academic Press: New York, 1982.
(4) Smith, J. V. *Chem. Rev.* **1988**, *88*, 149.
(5) Haushalter, R. C.; Mundi, L. A. *Chem. Mater.* **1992**, *3*, 31.
(6) Beltrán-Porter, D.; Beltrán-Porter, A.; Amorós, P.; Ibáñez, R.; Martínez, E.; Le Bail, A.; Ferey, G.; Villeneuve, G. *Eur. J. Solid State Inorg. Chem.* **1991**, *28*, 131, and references cited therein.
(7) Centi, G.; Trifiro, F.; Ebner, J. R.; Franchetti, V. M. *Chem. Rev.* **1988**, *88*, 55.
(8) Zubieta, J. *Comments Inorg. Chem.* **1994**, *16*, 153.
(9) Lii, K. H. *J. Chin. Chem. Soc.* **1992**, *39*, 569.
(10) Stein, A.; Keller, S. W.; Mallouk, T. E. *Science* **1993**, *259*, 1558.
(11) Marcos, M. D.; Amorós, P.; Beltrán, D.; Beltrán, A. *Solid State Ionics* **1993**, *63/65*, 96.
(12) Baes, C. F.; Mesmer, R. E. *The Hydrolisis of Cations*, Wiley: New York, 1976.

S0020-1669(96)00218-2 CCC: $12.00

by selective replacement of V(III) by Fe(III). In both cases, ethylenediamine (en) is used as "structural directing agent". The crystal structure and thermal behavior of the bimetallic open framework solid $[H_3N(CH_2)_2NH_3]_2[H_3N(CH_2)_2NH_2]$ $[Fe^{III}(H_2O)_2(V^{IV}O)_8$ $(OH)_4(HPO_4)_4(PO_4)_4]\cdot 4H_2O$ is presented.

Experimental Section

Sample Preparation. Synthesis of $[H_3N(CH_2)_2NH_3]_2$ $[H_3N(CH_2)_2NH_2][V^{III}(H_2O)_2(V^{IV}O)_8(OH)_4(HPO_4)_4(PO_4)_4]\cdot 4H_2O$ (1). A mixture of V (0.0293 g, 0.575 mmol), V_2O_5 (0.1921 g, 1.056 mmol), ethylenediamine (0.26 mL, 3.37 mmol), 85% H_3PO_4 (0.25 mL, 3.67 mmol), acetic acid (0.16 mL, 2.79 mmol), and water (9.52 mL, 528 mmol) was placed in a Teflon acid digestion bomb (23 mL, pH_i = 3.4), filled to 44% of its volume and heated at an external temperature of 200 °C for 48 h under autogeneous pressure. A dark-blue polycrystalline powder with a yield of 80% (based on vanadium) was separated from the mother liquor (pH_f = 3.9) by filtration, washed with water and acetone, and air-dried (Anal. Found: C, 4.16%, N, 4.98%; H, 2.83%; V, 26.81%; P, 14.51%. Calcd: C, 4.21%; N, 4.91%; H, 2.89%; V, 26.78%; P, 14.48%).

Synthesis of $[H_3N(CH_2)_2NH_3]_2$ $[H_3N(CH_2)_2NH_2]$ $[Fe^{III}(H_2O)_2(V^{IV}O)_8(OH)_4(HPO_4)_4(PO_4)_4]\cdot 4H_2O$ (2). The synthesis was similar to the above described for solid **1**. The hydrothermal reaction of V metal (0.0254 g), V_2O_5 (0.1821 g), $Fe(NO_3)_3\cdot 9H_2O$ (0.1480 g), ethylenediamine (0.26 mL), H_3PO_4 85% (0.25 mL), acetic acid (0.16 mL), and water (9.52 mL) in the optimized molar ratio 0.5:1:0.36: 3.37:3.67:2.79:528 (pH_i = 3.6) for 48 h at 200 °C and autogeneous pressure allowed us to obtain a gray-blue polycrystalline monophasic solid with a yield of 85% (based on vanadium). Compound **2** was separated by filtration (pH_f = 4.0), washed with water and acetone, and air-dried (Anal. Found: C, 4.17%; N, 4.92%; H, 2.83%; Fe, 3.29%; V, 23.73%; P, 14.50%. Calcd: C, 4.20%; N, 4.90%; H, 2.88%; Fe, 3.25%; V, 23.74%; P, 14.43%). Several small and well-formed blue crystals of **2** were obtained together with the polycrystalline sample. One crystal of **2**, suitable for single crystal diffraction techniques, was selected for the structural study. On the basis of X-ray powder diffraction analysis, both the single crystal and the gray-blue powder correspond to the same solid. The presence of Fe in the final solid was initially confirmed by X-ray fluorescence analysis. Moreover, microprobe analyses, both on powdered samples and selected single crystals, confirm the presence of Fe and the proposed formulation. Finally, in order to determine in a more conclusive way the Fe/V ratio, chemical analyses were carried out by means of atomic absorption spectrometry.

Analysis. Vanadium, iron, and phosphorus contents were determined, after dissolution of the solids in boiling concentrated hydrochloric acid, by atomic absorption spectrometry (Perkin-Elmer Zeeman 5000). Water and ethylenediamine were determined by elemental and thermogravimetric analyses.

Physical Measurements. X-ray fluorescence measurements have been performed using a Siemens SRS200 spectrometer working at 30 mA and 50 kV.

X-ray powder diffraction data were collected on a Siemens D501 automated diffractometer. Cu Kα radiation was selected with a graphite monochromator in the reflected beam. The patterns were collected in steps of 0.03° (2θ) over the angular range 2−70° (2θ) counting for 6 s per step.

To follow the course of the thermal evolution of compound **2**, we have used time resolved X-ray thermodiffractometric techniques. The diffractometer is equipped with a variable temperature device (Anton Paar HTK-10) working from room temperature to *ca.* 1200 °C. The powder patterns were recorded in steps of 0.05° (2θ) over the representative short angular range 5−20° (2θ) for 5 s per step. The temperature was increased by steps of 25 °C starting from room temperature up to *ca.* 400 °C. The diffraction patterns were analyzed numerically, and the relative percentage of solid **2** was determined from the thermal evolution of the integrated intensity of the well-isolated (200) Bragg peak.

Table 1. Crystallographic Data for Compound **2**

empirical formula	$C_6H_{48}N_6O_{50}P_8V_8Fe$
unit cell dimens	
a (Å)	14.383(3)
b (Å)	10.150(2)
c (Å)	18.355(4)
β (deg)	90.39(3)
V (Å^3)	2679.54(10)
Z	2
MW	1715.58
space group	$P2_1/n$
T (°C)	25
λ (Å)	0.710 73
dens (mg/m^3)	2.084
abs coeff(μ, mm^{-1})	1.95
final *R* indices (obsd data)	
R_1 (F)[a] (%)	7.19
R_{w2} (F^2)[b] (%)	22.66

[a] $R_1 = \sum||F_o| - |F_c||/\sum|F_o|$. [b] $R_{w2} = [\sum[w(F_o^2 - F_c^2)^2]/\sum[w(F_o^2)^2]]^{1/2}$.

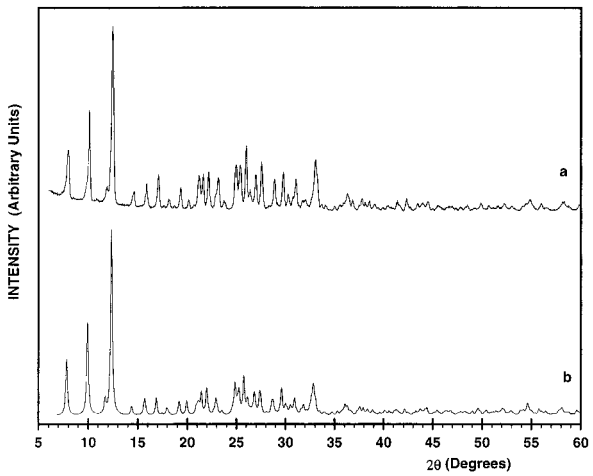

Figure 1. Experimental (a) and calculated (b) X-ray powder diffraction patterns of compound **1**.

Thermogravimetric studies were performed using a TGA-7 Perkin-Elmer instrument. Samples were heated up to 850 °C at 5° min^{-1} under flowing nitrogen. Both intermediate and final solids were characterized by means of X-ray powder diffraction and SEM.

SEM observations and energy dispersive X-ray emission (EDX) microprobe analysis were performed using a Hitachi 2500 microscope.

X-ray Crystallographic Study. A blue crystal (0.20 × 0.34 × 0.25 mm) was mounted on a thin glass fiber, and room temperature (25 °C) intensity data were collected on a RIGAKU AFC7R automated four-circle diffractometer using graphite monochromated Mo Kα radiation and an 18 kW rotating anode generator. Table 1 gathers the experimental conditions. Cell constants and an orientation matrix for data collection, obtained for a least squares refinement using the setting angles of 30 carefully centered reflections (θ = 10−15), correspond to a monoclinic cell, a = 14.383(3) Å, b = 10.150(2) Å, c = 18.355(4) Å, and β = 90.39(3)° (Z = 2). The conditions limiting possible reflections were consistent with the $P2_1/n$ space group, *i.e.*, solids **2** and **1** are isotypic (see Figures 1 and 2). The data were corrected for Lorentz and polarization effects. The structure was solved by direct methods using the SHELXTL program and all observed data.[14] Initial atom positions given by he direct methods and successive Fourier difference maps performed using the SHELX93 program[15] allow one to locate all the V, Fe, P, and O atoms forming the inorganic framework and the C and N atoms of one amine group. Several peaks, observed in the E-map calculations, near the inversion center, were consistent with the C and N atom positions of a second amine disordered over

(13) Livage, J.; Henry, M.; Sanchez, C. *Prog. Solid State Chem.* **1988**, *18*, 259.

(14) Sheldrick, G. M. *SHELXTL-Plus*, Release 4.1; Siemens Analytical X-ray Instruments Inc.: Madison, WI, 1991.

(15) Sheldrick, G. M. *SHELXL93*, Program for the Refinement of Crystal Structures, University of Göttingen: Göttingen, Germany, 1993.

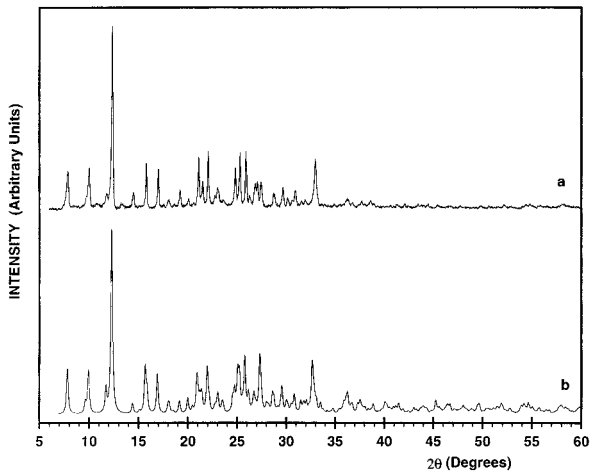

Figure 2. Experimental (a) and calculated (b) X-ray powder diffraction patterns of compound **2**.

two symmetry related positions. A strict 0.5 occupancy factor was fixed, and C−C and C−N constraints were used in further refinements. If we consider that this second amine is monoprotonated, electroneutrality is achieved, as occurs for the V(III)−V(IV) analogous derivative described in ref 16. Isolated peaks were assigned to oxygen water molecules. Their occupancy factors were fixed, taking into account chemical and thermal analysis. The occupation was subsequently distributed in accordance with the electronic density of the peaks in the difference Fourier map. Hydrogen atom locations were calculated, supposing ideal geometries, and their positions were refined with constraint in their distances, angles, and temperature factors. The final value of the residual was $R = 7.12\%$. The non-hydrogen atoms were refined anisotropically. The atomic coordinates are gathered in Table 2. Selected bond lengths and angles are listed in Table 3.

Results and Discussion

Synthesis: From Solution Chemistry to the Final Solids. In the past few years, new classes of molecular sieves based on phosphates of transition metals (mainly V and Mo) have been prepared by hydrothermal methods. Nevertheless, the chemistry underlying the synthesis of some of these compounds is not always well-established because the role of one or several reactants added *ad hoc*, such as organophosphonic acids, is not understood. However, different authors have stated that the presence of one determined organophosphonate reagent is required in order to obtain the desired oxovanadium phosphate. In the same way, different organic amines used as reactants do not appear in the final product, but a "templating effect" is attributed to them.[19−21] As stated above, other problems are the obtention of polyphasic products and the poor yields reached through the proposed procedures.[22]

In contrast to the usual, we have used V metal and V_2O_5 as vanadium sources, but always in the quantitative stoichiometric ratio required for the presence of all the vanadium as V(IV) ($V + 4VO_2^+ + 6H^+ \rightarrow 5VO^{2+} + 3H_2O$). The V(0):V(V) ratio used is 1:4 (or V(0):V_2O_5 = 1:2) in the case of the V(IV)−Fe(III) bimetallic compound **2** and 1:3.8 for compound **1**. Notwithstanding, several tentative syntheses carried out starting from the required V(0)/V(V) stoichiometric amounts led us, in all cases, to mixed valence V(IV)−V(V) phosphates. Taking into account the redox potentials of all of the species inside the reactor, the only one able to partially oxidize V(IV) is the oxygen present into the bomb, both in the void space and in the mother aqueous solution ($\epsilon°(O_2/H_2O) = 1.229$ V and $\epsilon°(VO_2^+/VO^{2+}) = 0.9994$ V). To avoid this problem, we added to the reaction vessel an additional species having a redox potential lower than that corresponding to the VO_2^+/VO^{2+} pair. We have successfully used acetic acid ($\epsilon°(CO_2/CH_3COOH) = 0.110$ V) as such a "catch" species, and similar results are obtained by using oxalic acid ($\epsilon°(CO_2/H_2C_2O_4) = -0.49$ V). The increase of pressure due to the CO_2 formation can be considered negligible.

In addition to redox problems, the key variable in order to control the formation of one or another phase (for a given vanadium concentration) is the pH of the starting solution. According to the literature,[12] it seems clear that, to avoid vanadium polymerization, the upper limit of the effective pH

Table 2. Atomic Coordinates ($\times 10^4$) and Equivalent Isotropic Displacement Parameters ($A^2 \times 10^3$) for **2**

	x	*y*	*z*	*U*(eq)[a]
V(1)	3411(2)	1838(2)	1040(1)	19(1)
V(2)	−2878(2)	3017(2)	−1965(1)	17(1)
V(4)	2531(2)	3485(2)	−1966(1)	16(1)
V(3)	−2531(2)	1389(2)	1073(1)	22(1)
Fe	0	0	0	43(1)
P(1)	1535(3)	6370(4)	−1990(2)	19(1)
P(2)	1647(3)	4282(3)	1867(2)	18(1)
P(3)	1834(3)	1436(4)	−693(2)	17(1)
P(4)	−1979(3)	1118(4)	−664(2)	20(1)
O(1)	3444(8)	2488(11)	1095(6)	35(3)
O(2)	3420(8)	3880(10)	−1485(5)	27(3)
O(3)	−3589(9)	1847(12)	1137(8)	55(4)
O(4)	−3892(8)	3183(10)	−1679(6)	28(3)
O(5)	−1753(9)	2932(10)	1271(5)	33(3)
O(6)	1574(7)	4885(9)	−1873(5)	21(2)
O(7)	2729(8)	1747(9)	−2435(5)	22(3)
O(8)	569(8)	6780(10)	−2255(6)	29(3)
O(9)	1522(7)	3245(9)	1280(5)	16(2)
O(10)	−2884(7)	1278(9)	−2456(5)	17(2)
O(11)	−2252(8)	4605(9)	−1600(5)	26(3)
O(12)	694(8)	4853(11)	2059(6)	38(3)
O(13)	1968(8)	2140(9)	29(5)	20(3)
O(14)	−2670(8)	−536(9)	852(5)	24(3)
O(15)	1711(7)	2495(9)	−1291(5)	19(3)
O(16)	945(8)	582(11)	−711(5)	32(3)
O(17)	2692(8)	−11(9)	817(5)	24(3)
O(18)	−2062(9)	2166(10)	−1259(5)	32(3)
O(19)	−2165(8)	1748(9)	71(5)	27(3)
O(20)	−978(8)	560(11)	−704(6)	29(3)
O(21)	2160(8)	1153(9)	2055(5)	26(3)
O(22)	2817(8)	4262(9)	−2937(5)	25(3)
O(23)	−29(9)	1747(14)	487(6)	53(4)
N(2)	−147(12)	2472(15)	−1801(9)	54(5)
C(2)	−275(19)	1837(21)	−2478(10)	67(7)
C(1)	117(20)	612(18)	−2602(11)	76(8)
N(1)	7(10)	−439(12)	−2075(7)	34(4)
C(3)	4673(103)	−535(200)	474(26)	420(134)
N(3)	5437(39)	46(70)	−40(42)	134(22)
N(4)	5518(19)	−1562(24)	1173(13)	29(6)
C(4)	4792(27)	−422(35)	1228(22)	52(11)
O(24)	−3440(35)	4732(47)	−101(25)	131(16)
O(25)	−1378(30)	5018(41)	118(22)	111(13)
O(26)	0	5000	0	212(40)
O(27)	4856(33)	13421(46)	9909(24)	127(15)
O(28)	−2428(33)	4656(40)	−48(20)	25(10)

[a] *U*(eq) is defined as one-third of the trace of the orthogonalized $\mathbf{U}_{ij}$ tensor.

(16) Soghomonian, V.; Chen, Q.; Haushalter, R. C.; Zubieta, J. *Angew. Chem., Int. Ed. Engl.* **1993**, *32*, 610.
(17) Soghomonian, V.; Chen, Q.; Haushalter, R. C.; Zubieta, J.; O'Connor, C. J. *Science* **1993**, *259*, 1596.
(18) Soghomonian, V.; Haushalter, R. C.; Chen, Q.; Zubieta, J. *Inorg. Chem.* **1994**, *33*, 1700.
(19) Zhang, Y.; Clearfield, A.; Haushalter, R. C. *J. Solid State Chem.* **1995**, *117*, 157.
(20) Haushalter, R. C.; Wang, Z.; Thompson, M. E.; Zubieta, J.; O'Connor, C. J. *J. Solid State Chem.* **1994**, *109*, 259.
(21) Haushalter, R. C.; Chen, Q.; Soghomonian, V.; Zubieta, J.; O'Connor, C. J. *J. Solid State Chem.* **1994**, *108*, 128.
(22) Soghomonian, V.; Chen, Q.; Haushalter, R. C.; Zubieta, J. *Chem. Mater.* **1993**, *5*, 1595.

Table 3. Selected Bond Lengths (Å) and Angles (deg) for **2**

V(1)−O(1)	1.629(13)	V(1)−O(17)	1.963(9)
V(1)−O(9)	1.968(10)	V(1)−O(13)	1.980(9)
V(1)−O(21)	2.025(9)	V(2)−O(4)	1.563(11)
V(2)−O(18)	1.946(11)	V(2)−O(11)	1.963(10)
V(2)−O(10)	1.981(9)	V(2)−O(21)$^{(1)}$	1.987(9)
V(4)−O(2)	1.600(11)	V(4)−O(7)	1.984(9)
V(4)−O(6)	1.987(10)	V(4)−O(15)	1.990(9)
V(4)−O(22)	1.993(9)	V(3)−O(3)	1.595(13)
V(3)−O(19)	1.951(10)	V(3)−O(5)	1.958(11)
V(3)−O(22)$^{(2)}$	1.994(10)	V(3)−O(14)	2.005(10)
Fe−O(16)	1.981(9)	Fe−O(16)$^{(3)}$	1.981(9)
Fe−O(23)$^{(3)}$	1.986(14)	Fe−O(23)	1.986(14)
Fe−O(20)	1.987(11)	Fe−O(20)$^{(3)}$	1.987(12)
P(1)−O(6)	1.523(10)	P(1)−O(8)	1.527(12)
P(1)−O(5)$^{(4)}$	1.528(11)	P(1)−O(7)$^{(5)}$	1.548(10)
P(2)−O(11)$^{(4)}$	1.510(11)	P(2)−O(9)	1.517(10)
P(2)−O(10)$^{(6)}$	1.521(10)	P(2)−O(12)	1.531(12)
P(3)−O(13)	1.518(10)	P(3)−O(14)$^{(3)}$	1.539(11)
P(3)−O(15)	1.545(10)	P(3)−O(16)	1.545(12)
P(4)−O(19)	1.520(10)	P(4)−O(18)	1.528(10)
P(4)−O(17)$^{(3)}$	1.546(11)	P(4)−O(20)	1.549(12)
N(2)−C(2)	1.41(2)	C(2)−C(1)	1.39(3)
C(1)−N(1)	1.45(2)	C(3)−C(4)	1.40(3)
C(3)−N(3)	1.57(3)	N(4)−C(4)	1.56(3)

O(1)−V(1)−O(17)	102.2(5)	O(1)−V(1)−O(13)	106.5(5)
O(17)−V(1)−O(13)	91.1(4)	O(13)−V(1)−O(21)	149.0(5)
O(4)−V(2)−O(18)	112.6(5)	O(4)−V(2)−O(11)	102.9(5)
O(18)−V(2)−O(11)	82.2(4)	O(18)−V(2)−O(21)$^{(1)}$	140.5(5)
O(2)−V(4)−O(7)	110.3(5)	O(7)−V(4)−O(6)	140.8(5)
O(7)−V(4)−O(15)	84.7(4)	O(2)−V(4)−O(22)	103.1(5)
O(3)−V(3)−O(5)	107.3(6)	O(19)−V(3)−O(5)	82.4(4)
O(19)−V(3)−O(22)$^{(2)}$	148.6(5)	O(3)−V(3)−O(14)	101.9(6)
O(16)−Fe−O(23)$^{(3)}$	87.3(5)	O(16)−Fe−O(20)	88.4(5)
O(23)$^{(3)}$−Fe−O(20)$^{(3)}$	91.2(5)	O(6)−P(1)−O(8)	110.3(6)
O(6)−P(1)−O(7)$^{(5)}$	108.4(6)	O(11)$^{(4)}$−P(2)−O(10)$^{(6)}$	107.0(6)
O(9)−P(2)−O(10)$^{(6)}$	111.8(5)	O(13)−P(3)−O(16)	112.6(6)
O(15)−P(3)−O(16)	106.5(6)	O(19)−P(4)−O(20)	111.4(6)
O(18)−P(4)−O(20)	106.8(6)		

[a] Symmetry transformations used to generate equivalent atoms: (1) $x - {}^1/_2, -y + {}^1/_2, z - {}^1/_2$; (2) $x - {}^1/_2, -y + {}^1/_2, z + {}^1/_2$; (3) $-x, -y, -z$; (4) $-x, -y + 1, -z$; (5) $-x + {}^1/_2, y + {}^1/_2, -z - {}^1/_2$; (6) $x + {}^1/_2, -y + {}^1/_2, z + {}^1/_2$.

working range is, approximately, 4.5−5.0. In fact, all of the syntheses described in the bibliography were carried out at pH values ranging from 1.0 to 4.5.[8] The synthesis of oxovanadium phosphates that contain additional inorganic cations are usually performed at very low pH values (∼1−2).[23−25] The resulting solids show a typical lamellar morphology related to that of the well-known $VOPO_4 \cdot 2H_2O$.[26] However, when organic species (such as amines) are involved in the synthesis (and, in the reaction products), a significant pH increase of the starting solution is expected. In our opinion, the role played by the other "required" reagents such as organophosphonic acids (that do not appear in the final solids) is only to adjust the pH value to the adequate range (∼3−4). Under these pH conditions, complex corrugated layered or microporous derivatives are obtained,[8] a result that has also been attained in some cases by working with inorganic cations.[9]

The synthesis of solid **1** has been done by being careful to set the above variables. The V(0):V(V) molar ratio in the starting solution was 1:3.8; the pH was adjusted to 3.5 by adding the required amounts of the reagents en, H_3PO_4 and CH_3COOH (to avoid V(IV) oxidation), but any other reagent (like the usual organophosphonic acids) was excluded. Compound **1** is obtained as a monophasic product, and the reaction yield (measured with respect to the total amount of vanadium in the starting solution) is close to 85%. The synthesis of the isostructural Fe(III) containing derivative (**2**) is practically coincident. The only remarkable differences are the value of the V(0):V(V) initial ratio, 1:4, and the presence in the starting solution of the required quantity of Fe(III) to stoichiometrically replace all V(III). In the resulting phosphate network, all vanadium atoms are present as VO^{2+} cations. The fact that iron can fully replace vanadium to give the new monophasic product **2** isostructural to **1** (reaction yield 85%) supports our hypothesis about the essential role played by the strict control of the vanadium oxidation state in the final solid.

On the other hand, the dramatic structural changes in the A−V−P−O series that are induced by relatively small pH variations in the starting solutions reinforce the above considerations concerning the influence of the hydrolytic processes on the nature of the resulting network. It is in this context where a simple model, such as the PCM, becomes an useful tool in order to rationalize the preparative chemistry.

Simple Models to Complex Materials. The PCM, as formulated by Livage et al.,[13] is a derivation of the electronegativity equalization Sanderson's principle, and it is also based on the idea that species showing similar electronegativity coexist without reaction among them. The model is intended to calculate the atomic partial charge in any species in order to predict its chemical reactivity, given that (1) it is usually assumed that the electronegativity χ_i of an atom changes linearly with its partial charge and (2) a partial electron transfers occurs when two atoms combine; the net charge transfer stops in the moment that the electronegativity of each atom reaches a given $\bar{\chi}$ value.

Whereas Livage's model starts from Pauling's electronegativity scale, a more accurate representation can result from the use of the Mulliken−Jaffé scale (that, for different atoms, assumes different electronegativity variation rates with the partial charge). Accordingly, the basic equations of the PCM[13] can be restated as follows:

(1) From Sanderson's principle, the charge transfer should stop when the χ_i value of each atom becomes equal to the mean electronegativity $\bar{\chi}$, given now by

$$\bar{\chi} = \frac{z + \sum_i (p_i (a_i / b_i))}{\sum_i (p_i / b_i)} \qquad (1)$$

where a_i and b_i are the two electronegativity parameters in the Mulliken−Jaffé scale, p_i corresponds to the stoichiometry of the ith atom in the compound, and z is the total charge of the ionic species.

(2) Then, it is possible to calculate the δ_i partial charge on each atom as

$$\delta_i = \frac{\bar{\chi} - a_i}{b_i} \qquad (2)$$

On the basis of the calculated δ_i values, it is possible to predict the progress of the hydrolytic and condensation processes of the chemical species in solution. Thus, for transition metal ions in noncomplexing aqueous solutions, the general equations to be considered are

(23) Kang, H. Y.; Lee, W. C.; Wang, S. L.; Lii, K. H. *Inorg. Chem.* **1992**, *31*, 4743.
(24) Lii, K. H.; Wu, L. S.; Gau, H. M. *Inorg. Chem.* **1993**, *32*, 4153.
(25) Wang, S. L.; Kang, H. Y.; Cheng, C. Y.; Lii, K. H. *Inorg. Chem.* **1991**, *30*, 3496.
(26) Tietze, H. R. *Aus. J. Chem.* **1981**, *34*, 2035.

$$[M{-}OH_2]^{z+} \leftrightarrow [M{-}OH]^{(z-1)+} + H^+ \leftrightarrow [M{-}O]^{(z-2)+} + 2H^+ \quad (3)$$

$$[M(OH_2)_N]^{z+} + 2pH_2O \leftrightarrow [M(OH)_p(OH_2)_{(N-p)}]^{(z-p)+} + pH_5O_2^+ \quad (4)$$

The first one simply implies a partial charge transfer from the water molecule to the empty *d* orbitals of the transition metal atoms. This results in a certain increase of the positive partial charge on the H atoms, and, consequently, the water molecule as a whole becomes more acidic. The second equation, which refers to processes happening under acidic conditions, implies the cleavage of the O−H bond due to the metal atom's large polarization. This occurs as long as $\delta(OH) > 0$ in the hydrated precursor. The limiting condition, $\delta(OH) = 0$, leads to the following relations:

$$\bar{\chi} = \chi(OH) = 10.24 \quad (5)$$

$$p = 1.32\left[\frac{a_M - \bar{\chi}}{b_M} + z - 0.24n\right] \quad (6)$$

p being the estimated hydrolysis progress, i.e., the value of this coefficient in eq 6. If $p < 0$, the precursor species does not exhibit any acidic behavior and a base such as OH^- must be added in order to initiate the hydrolysis. On the other hand, when $\delta(OH) < 0$, condensation processes occur after the initial hydrolytic ones. As the hydrolysis−condensation processes progress, the partial charge on the oxygen atoms (H_2O, OH^-, and O^{2-}) linked to the metal ions changes; it eventually becomes null, and then the process stops.

On the other hand, in the presence of anions having significant complexing ability, both the nature of the molecular precursors in solution and their reactivity toward hydrolysis and condensation can result strongly modified. The basic ideas concerning these equilibria are adequately developed in the Livage's work.[13]

Hydrolysis and Condensation of Oxovanadium(IV) and Iron(III): Application of the PCM Model. As stated above, these ideas can be used to organize the experimental results and to make reasonable predictions in the search for adequate synthetic strategies. According to the literature data, the V(IV) species that predominates in aqueous solution at low pH values is $VO(H_2O)_5^{2+}$ (species **I**).[12] As the pH increases, hydrolysis and condensation lead to $VO(OH)(H_2O)_4^+$ (species **II**) and $(VO)_2(OH)_2(H_2O)_6^{2+}$ (species **III**), which are soluble.[12] Olation is fast, and the predominant species in the absence of coordinating anions is the stable dimer **III.** This result is in good agreement with PCM predictions:[13] the partial charge on the OH group is very low, and the condensation in acidic medium stops at this species. Figure 3 shows the distribution diagram for these species at 25 °C (from data in ref 12). The species formed in basic media have not been studied in detail. Notwithstanding, the Schlemper fully oxolated polyanion $(VO)_{18}O_{24}^{12-}$ (species **IV**)[27] exists in the pH range from 9 to 13, and, at low vanadium concentrations, the monomeric anion $VO(OH)_3^-$ has been detected.[12]

Ferric ion hydrolyzes readily. The hydrolysis begins around pH 2, and several mononuclear and binuclear species result as the pH increases. However, in the pH conditions normally used to prepare organic species containing oxovanadium phosphates, the majority species is the aquocation $[Fe(H_2O)_6]^{3+}$ (labeled as the 1:0 species), even though a small quantity of $[Fe(OH)(H_2O)_5]^{2+}$ (1:1 species) can also be present.[12]

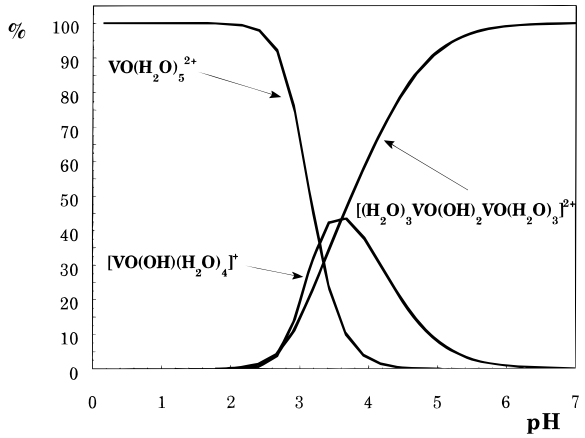

Figure 3. Distribution diagram of the oxovanadium(IV) species. Species **I**−**III** have been considered.

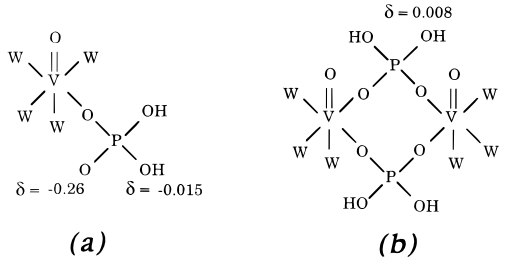

Figure 4. Schematic representation of the first complex 1:1 entity formed at very low pH values, $[VO(H_2O)_4(H_2PO_4)]^+$ (a), and the cyclic molecular cationic precursor $[(VO)_2(H_2O)_6(H_2PO_4)_2]^{2+}$ (b).

As mentioned above, these processes may be substantially altered by the presence in the solution of other complexing ions, such as that which occurs in the case of phosphate oxoanions. In practice, the ability of polydentate ligands (like phosphate groups) to connect the cationic entities entails the possibility of the formation of polymeric species.

We see how the model works in this case. At very low pH values (≈1), the initially predominant ions in solution are species **I**, $VO(H_2O)_5^{2+}$, and the dihydrogenophosphate anions, $H_2PO_4^-$. By entering $H_2PO_4^-$ entities in the coordination sphere of the vanadyl aquoions, the first possible complex entity formed would be the 1:1 species, $[VO(H_2O)_4H_2PO_4]^+$. As schematized in the Figure 4a, calculations from equations of the PCM indicate that the resulting partial charge on the oxygen atoms of the phosphate ligand is negative and very high. Hence, condensation with an equivalent entity by means of a nucleophilic substitution mechanism is feasible. This process would allow the formation of the cyclic molecular precursor, $[(VO)_2(H_2O)_6(H_2PO_4)_2]^{2+}$, schematized in Figure 4b. In fact, this last precursor constitutes the basic motif appearing in a great number of oxovanadium phosphates: the di-μ-(O,O′)-phosphate bridge.[6,9] According to the PCM ideas, the dimeric entity (in which $\delta(OH) > 0$) should hydrolyze and then condensate again. In this way, through iterative hydrolysis and condensation reactions, one could understand the formation of the 2-D anion $[VO(H_2O)PO_4]_n^{n-}$, precursor of all the lamellar solids showing the typical structural network derived from that of $VOPO_4 \cdot 2H_2O$.[28] An hydrolysis−condensation sequence like this should be effective regardless of the nature (organic or inorganic) of the charge compensating guest cations. A case in point is that of the piperacinium derivative $(H_2NC_4H_8NH_2)[(VOPO_4)_2]$,[18,29] whose synthesis has been performed in strongly acidic medium.

(27) Johnson, G. K.; Schlemper, E. O. *J. Am. Chem. Soc.* **1978**, *100*, 3645.
(28) Roca, M. Tesis de Licenciatura, Universitat de València, 1995.
(29) Riou, D.; Ferey, G. *Eur. J. Solid State Inorg. Chem.* **1994**, *31*, 25.

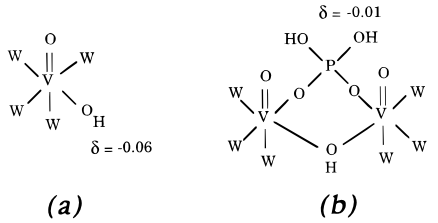

Figure 5. Species **II**, $VO(OH)(H_2O)_4^+$ (a), and phosphate precursor species, obtained through condensation of species **I** and **II** at intermediate pH values, observed in most oxovanadium(IV) phosphates templated by organic molecules, $[(VO)_2(H_2O)_6(OH)(H_2PO_4)]^{2+}$ (b).

On the other hand, with exception being made of the piperacinium derivative, all of the known oxovanadium phosphates that include organic cations have been synthesized at slightly higher pH values. In the usual pH working range (3−4), although the $H_2PO_4^-$ anions and the aquocation **I** predominate, the amount of the aquocation **II** is not negligible (its relative concentration depending on the pH). Thus, besides the formation of di-μ-(O,O′)-phosphate bridges considered above, additional hydrolysis condensation sequences involving species **II** could lead to new molecular precursors. In other words, although other possibilities exist, it does not seem wild to assume that the predominant complex 1:1 species $[VO(H_2O)_4H_2PO_4]^+$ condensate two by two to give di-μ-(O,O′)-bridges (Figure 2b); in a parallel way, it reacts with the minority **II** aquocations ($[(VO)_2(H_2O)_8(OH)]^{3+}$) to give a different cationic precursor, $[(VO)_2(H_2O)_6(OH)H_2PO_4]^{2+}$, involving both hydroxo and μ-(O,O′)-phosphate bridges. Really, this last entity, schematized in Figure 5, is frequently observed in oxovanadium phosphates that contain organic cations.[8] The PCM based calculations lead to an estimated δ(OH) value of −0.01 for $[(VO)_2(H_2O)_6(OH)H_2PO_4]^{2+}$, and, consequently, successive condensation reactions are expected. Depending on the way through which these reactions progress, one or another structural motif can result. Obviously, the PCM is unable to predict the structure of the final compound. At first glance, the ultimate nature of the solid network might be controlled by the peculiarities of the structural directing agent, and factors such as the charge, shape, and dimensions of the organic species (cation) might be determinant. Both ionic and hydrophilic−hydrophobic interactions in these solids are responsible of the final crystal packing. Although it should be possible to speculate about strategies to induce the incorporation of the organic groups, in our opinion, the point concerning the design of specific network types remains (up to date) uncontrolled, regardless of the care payed for a judicious choice of the reaction conditions and organic structural directing agents.

The recent isolation of two ethylenediamine containing phosphates that show topological similarities, namely, $(H_3N(CH_2)_2NH_3)_2(H_3N(CH_2)_2NH_2)[V^{III}(H_2O)_2(V^{IV}O)_8(OH)_4(HPO_4)_4(PO_4)_4]\cdot 4H_2O$[16] (compound **1**) and $(H_3N(CH_2)_2NH_3)_4[V^{III}(H_2O)_2(V^{IV}O)_6(OH)_2(HPO_4)_3(PO_4)_5]\cdot 3H_2O$ (compound **3**),[30] provide us with a nice example about the pH influence. Both compound **1** and the isostructural Fe(III)−V(IV) bimetallic derivative (compound **2**) have been obtained at relatively high pH values (≈3.5−4). Their structural networks are built up from $[(VO)_2(H_2O)_6(H_2PO_4)_2]^{2+}$ (Figure 4b) and $[(VO)_2(H_2O)_6(OH)(H_2PO_4)]^{2+}$ (Figure 3b) units. In contrast, compound **3** is obtained at slightly lower pH values. Hence, the number of hydroxo−phosphate bridges decreases. This difference induces stoichiometric changes in their respective formulations. Thus, whereas the compound described by Soghomonian et al.[16] (whose obtention as monophasic product is reported in this work, compound **1**) has a V:P molar ratio equal to 9:8, in the solid described by Zhang et al. (compound **3**)[30] this value is 7:8. Both compounds present channels of similar dimensions, but as the hydroxo−phosphate bridges give rise to a higher connectivity of the metallic polyhedra, the V:P molar ratio in compound **1** results higher than that of compound **3**. Obviously, changes in the respective stoichiometries of protonated phosphates and amines are necessary in order to maintain electroneutrality.

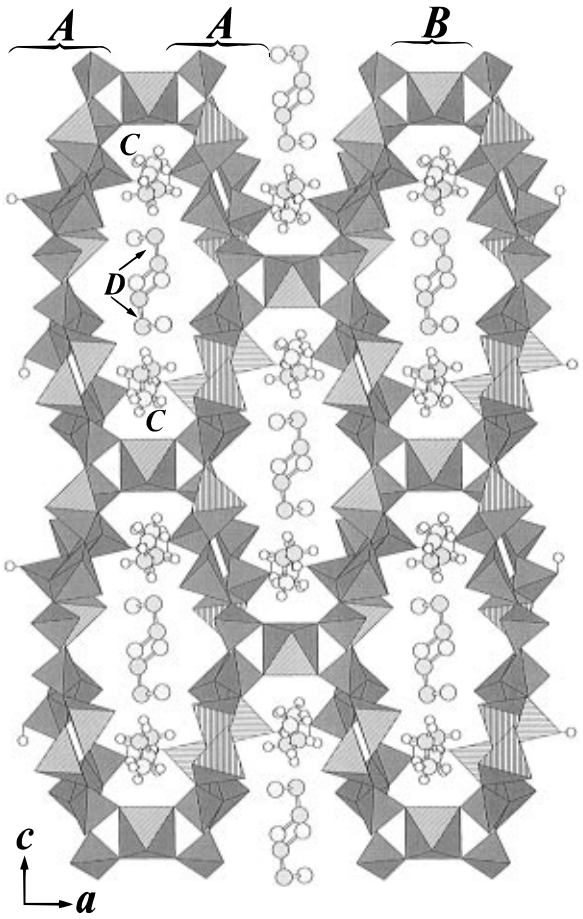

Figure 6. Projection along (010) of the crystal structure of compound **2**. (A) V−P−O layers; (B) FeO_6 octahedra. The large 18.4-Å-type channels, in which en molecules are located, are shown ((C) non-disordered en). The amine located in the center of the channel corresponds to the disordered guest amine (D).

Another interesting example of the pH influence is furnished by the formation of up to three different piperacine derivatives. At very low pH values (≈1−2) the above mentioned phosphate $[H_2NC_4H_8NH_2][(VOPO_4)_2]$[18,29] and the solid $[H_2NC_4H_8NH_2]_2[(VO)_3(HPO_4)_2(PO_4)_2]\cdot H_2O$[18] are obtained. These show a lamellar structure related to that of $VOPO_4\cdot 2H_2O$, and there are not hydroxo species present in their structures. The basic structural unit is constituted by di-μ-(O,O′)-phosphate bridges. On the other hand, at slightly higher pH conditions (≈3), condensation between species **I** and **II** occurs and hydroxo bridges between vanadium atoms result, as can be observed in $[H_2NC_4H_8NH_2][(VO)_4(OH)_4(PO_4)_2]$.[31]

Description of the Structure of Compound 2. Shown in Figures 6 and 7 are two projections of the structure of the title compound along the (010) and (100) directions. The structure closely resembles those found for zeolitic materials. Regarding its general features, the intricate 3-D framework may formally

(30) Zhang, Y.; Clearfield, A.; Haushalter, R. C. *Chem. Mater.* **1995**, *7*, 1221.

(31) Soghomonian, V.; Chen, Q.; Zhang, Y.; Haushalter, R. C.; O'Connor, C. J.; Tao, C.; Zubieta, J. *Inorg. Chem.* **1995**, *34*, 3509.

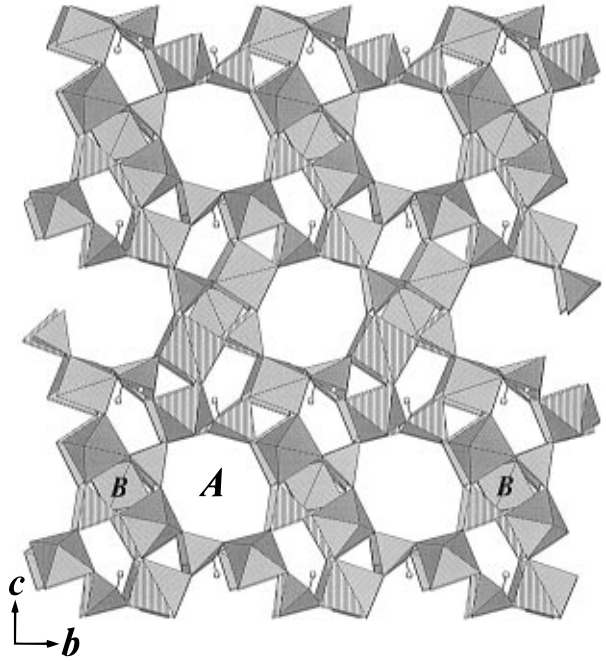

Figure 7. View of the crystal structure of compound **2** along the (100) direction showing the eight member channels (A) in which uncoordinated water molecules are placed. (B) FeO_6 octahedra.

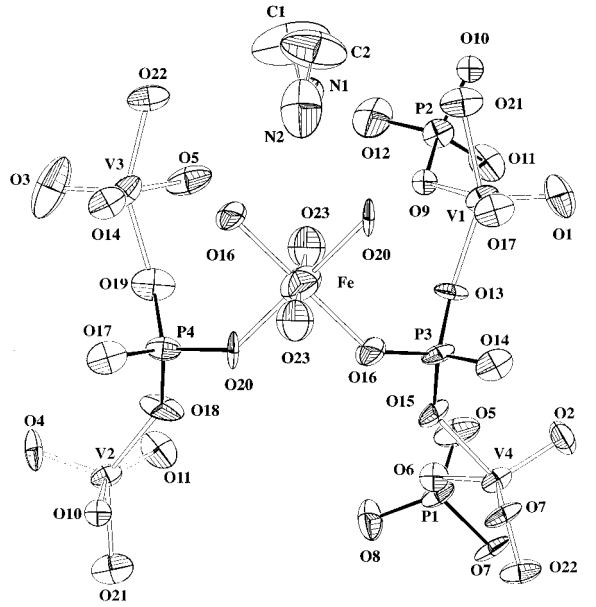

Figure 8. ORTEP view for compound **2** showing a representative structural portion. Thermal ellipsoids are at the 75% probability level.

be described as constituted by $V^{IV}O_5$ square pyramids, $Fe^{III}O_6$ octahedra, and PO_4^{3-} and HPO_4^{2-} tetrahedral groups. This inorganic network delimits three kinds of channels (running along the three spatial directions), in which organic species and water molecules are located.

The coordination octahedron formed by the oxygen atoms around the vanadium atoms in **2** shows the characteristic anisotropic bonding scheme observed in other oxovanadium(IV) derivatives (see Figure 8). Three equatorial oxygen atoms are shared with three different phosphate groups, and the remaining one corresponds to an hydroxo bridge between metallic atoms. The apical V−O bond, directed to the channels, corresponds to the oxovanadium group. The $V(2)O_5$ and $V(3)O_5$ square pyramids show a notable distortion and can be described as distorted trigonal bipyramids.

Table 4. Bond Valence Analysis of Compound **2** (in Valence Units)

	V(1)	V(2)	V(3)	V(4)	Fe	P(1)	P(2)	P(3)	P(4)	Σ
O(1)	1.52									1.52
O(2)			1.65							1.65
O(3)				1.67						1.67
O(4)		1.82								1.82
O(5)				0.63		1.23				1.86
O(6)			0.58			1.25				1.83
O(7)			0.58			1.16				1.74
O(8)						1.23				1.23
O(9)	0.61						1.27			1.88
O(10)		0.59					1.25			1.84
O(11)		0.62					1.29			1.91
O(12)							1.22			1.22
O(13)	0.59							1.19		1.78
O(14)				0.55				1.23		1.78
O(15)			0.57					1.25		1.82
O(16)					0.55 (×2)			1.16		1.71
O(17)	0.62								1.17	1.79
O(18)		0.65							1.23	1.88
O(19)				0.64					1.26	1.90
O(20)					0.54 (×2)				1.16	1.70
O(21)	0.52	0.58								1.10
O(22)			0.57	0.57						1.14
O(23)					0.54 (×2)					0.54
Σ	3.86	4.26	3.95	4.06	3.26	4.87	5.03	4.83	4.82	

The iron atom is located at the inversion center and its coordination environment is completed by six oxygen atoms forming a regular octahedron. Four oxygen atoms are shared with phosphate groups, and the remaining ones correspond to coordinated water molecules.

The bond valence analysis[32] has been carried out with utilization of the EUTAX program,[33,34] using the Brown equation, $s = \exp(R - R_0/B)$ ($R_0 = 1.784$ for V, $R_0 = 1.759$ for Fe, and $R_0 = 1.604$ for P; the same B value, 0.37, is used for all atoms). Such an analysis (see Table 4) provides a better understanding of the structure in that it concerns details of the cationic coordination, the location of water molecules and hydroxo groups, and the hydrogen bonding scheme. The result of this analysis, without taking into account the H atoms, shows a quite good agreement with the expected valence values for V, Fe, P, and five oxygen atoms (O(5), O(9), O(11), O(18), and O(19)). Oxygen atoms O(8), O(12), O(21), and O(22) show deficient valence values comprised between 1.1 and 1.2 valence units. These characteristic deficits correspond to O−H bonds of hydroxo groups, HPO_4 entities, or water molecules. On the other hand, the relatively low valence values of the remaining oxygen atoms are typical of noncomputed hydrogen bonding interactions.

The vanadium and phosphorous polyhedra form undulating layers running along the *bc* plane (see Figure 6). Such a connectivity delimits circular channels with a cavity diameter of 7.2 Å (Figure 7). These channels are described as domed rings made up of eight polyhedra: four VO_5 square pyramids, two HPO_4^{2-} groups, and two PO_4^{3-} tetrahedra (Figure 7). These rings are amphiphilic: the four less polar oxovanadium groups are on one side of the mean plane of the ring and four P−O groups are on the opposite side. Two of these four P−O groups are strongly polar PO−H entities. The eight member rings are stacked along the *b* axis and show the same V═O and P−O bond orientation. Each ring is surrounded by six other rings describing a hexagonal packed array.

The connectivity between the mentioned layers is provided through the FeO_6 octahedra. The resulting 3-D framework

(32) Brown, I. D. *Acta Crystallogr.* **1992**, *B48*, 553.
(33) Brese, N. E.; O'Keeffe, M. *Acta Crystallogr.* **1991**, *B47*, 192.
(34) O'Keeffe, M.; Brese, N. E. *J. Am. Chem. Soc.* **1991**, *113*, 3226.

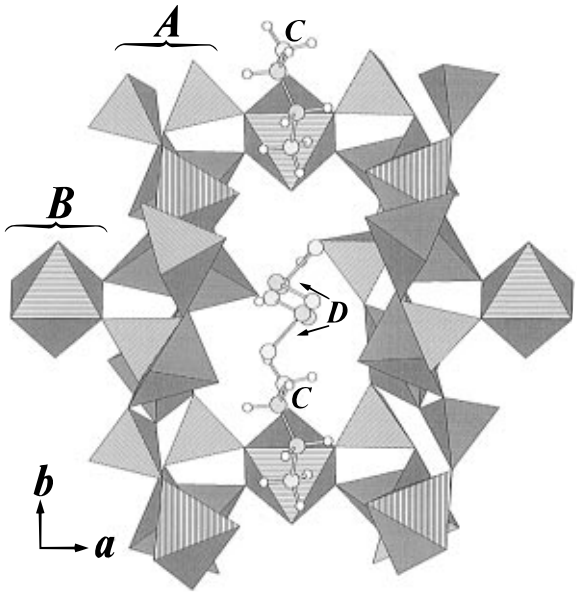

Figure 9. Schematic representation of the intermediate 10.5-Å-type channels running along the *c* direction: (A) V−P−O layers; (B) FeO_6 octahedra. Both the ordered (C) and disordered (D) ethylenediamine molecules are represented. The organic ethylenediamine species are located in the intercrossing channel system described by the big channels of 18.4 Å of diameter and the channels represented in this figure.

delimits the remaining two types of channels, which have diameters of 18.4 (Figure 6) and 10.5 Å (Figure 9), and run along the (010) and (001) directions, respectively.

The noncoordinated water molecules are located inside the tunnel running along the (100) direction, while the channels along *b* and *c* axes are occupied by ethylenediammonium cations. The amine disposition is governed by the hydrophobic−hydrophilic interactions which result in a connectivity pattern working for the segregation of polar and nonpolar cavities within the lattice. Since V═O moieties are considerably less polar than phosphate groups, the tendency of oxovanadium groups to encapsulate organic species should be enhanced. This principle has been successfully exploited in the synthesis of several organically templated phosphate derivatives. Dealing with the title compound, the nondisordered amines are located inside the great cavities of 18.4 Å of diameter. As shown in Figure 6, two diprotonated ethylenediamine molecules are encapsulated in each 18.4-Å-type channel, and they are displaced from the center in order to satisfy the hydrophobic−hydrophilic interactions. Hence, the polar NH_3^+ ends of the organic cations are situated close to the polar PO−H groups (d(N(1)−O(8)) = 2.955 Å and d(N(2)−O(12)) = 2.865 Å) in order to maximize hydrogen bonding interactions, while the less polar carbon backbones of the organic templates are near the oxovanadium bonds (d > 3.2 Å). The disordered monoprotonated amine cation, N(3)−C(3)−C(4)−N(4), is located at the center of the interconnected 18.4- and 10.5-Å-type channels. The charged end, N(4), as could be expected, is close to a PO−H group (d(N(4)−(O(8)) = 2.895 Å).

With respect to the role played by the organic species, we have used along this paper the term template in a wide sense. Actually, a symmetry matching between the symmetry elements of the organic guest molecule and the crystallographic symmetry of the inorganic lattice should exist in order to strictly consider an interaction between organic and inorganic species as a template effect.[12] It is not necessary, however, that the inorganic network adopts the full symmetry of the template molecules. In fact, the number of examples in which the strict template

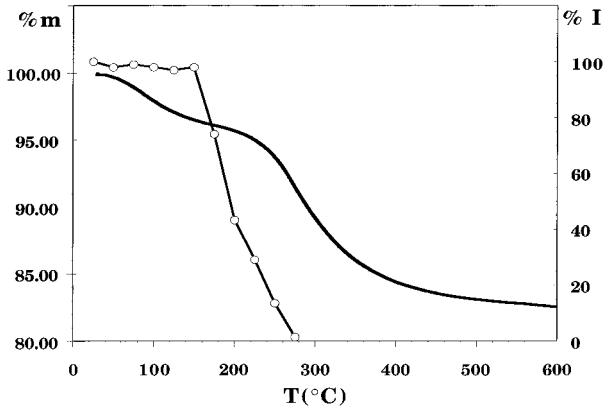

Figure 10. Thermogravimetric curve (—) and X-ray thermodiffractometry (○—○) of compound **2**. Small open circles represent the relative intensity of the reference peak for compound **2**.

symmetry effect occurs is scarce, and only recently it has been described as a case in point concerning the crystal structure of a oxovanadium(IV) phosphate containing piperazine dications.[35]

Thermal Behavior. Besides the basic interest of materials having open networks such as that of the title compound, their final applicability as sorbents or catalysts will depend on the accessibility of chemicals to the inner part of the micropores. This usually implies the need for template removal, which generally is accomplished by calcination.[10] Hence, we have carried out the study of the thermal evolution of the title compound.

Figure 10 shows the TG curve of compound **2**. From this, the following observations can be made: (a) no stable intermediates are evidenced in the course of the thermal evolution; (b) a weight loss of 4.02% is observed in the temperature range 73−196 °C and can be attributed to the noncoordinated water molecules evolution; (c) this first step is partially superimposed to the amine and coordinated water molecule elimination, a result which makes it difficult to assign unambiguously weight losses to individual reaction steps; (d) the second weight loss in the *ca.* 196−545 °C temperature range corresponds to the evolution of both coordinated water molecules and organic species (12.85%).

In order to get complementary information, we have used time-resolved X-ray thermodiffractometry. Figure 10 shows, simultaneously to the TG curve, the thermal evolution of the integrated intensity of the (200) Bragg peak. Its intensity remains practically unchanged up to *ca.* 150 °C. This fact indicates that the long-range order in this structure is maintained during the noncoordinated water molecule evolution. Between *ca.* 175 and 225 °C, the (200) peak collapses rapidly, disappearing completely at 250 °C during the amine elimination. The evolution of organic cationic species as $^+H_3N{-}CH_2{-}CH_2{-}NH_3^+$ requires moderately high temperatures, and the structure collapses as soon as the template is removed. After amine evolution an amorphous solid is obtained.

On the other hand, as shown by the SEM images (Figure 11), the crystal morphology of compound **2** remains unchanged even during the pyrolytic processes that yield the amorphous solid. Micrographs in Figure 11a,b clearly show the homogeneous particle size and the platelike shape of microcrystals, grouped in spherical aggregates. This result should not be ignored, but further porosimetry analysis is required in order to evaluate its possible relevance. At higher temperature, a syntherization process occurs (associated to the final weight loss)

(35) Bu, X.; Feng, P.; Stucky, G. D. *J. Chem. Soc., Chem. Commun.* **1995**, 1337.

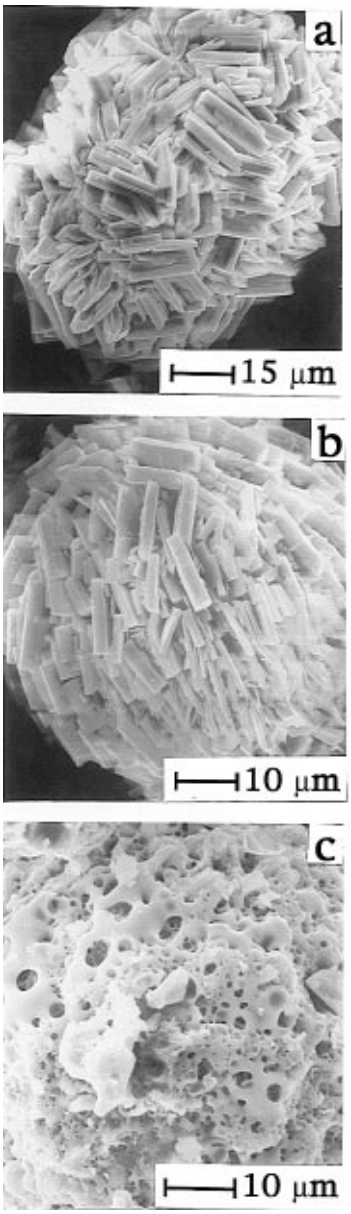

Figure 11. SEM images of compound **2** before heating (a), after amine evolution (≈400 °C) (b), and after heating at high temperature (≈800 °C) (c).

probably due to complex condensation reactions among phosphate and/or hydroxo groups (see Figure 11c).

Finally, to investigate the reversibility of the water insertion process in the inorganic lattice, we approached the study of the dehydration/rehydration reactions by means of thermal analysis. Thermogravimetric multiramp experiments have been performed by using a temperature profile defined by four consecutive steps: (a) a 3 °C min^{-1} heating ramp, (b) a 60 min dwell at 160 °C, (c) a −3 °C min^{-1} cooling ramp, and (d) a 200 min dwell at room temperature. The two last steps have been carried out under an H_2O saturated argon flowing atmosphere in order to rehydrate the sample. The thermal evolution is represented in Figure 12. Dehydration begins at low temperature (65 °C). When the sample is cooling, the rehydration process begins at 110 °C and the sample weight increases rapidly at room temperature. No complete rehydration is achieved. Factors such as the diffusion process along the moderately big microcrystals and the presence of cationic organic species blocking the channels cooperate to only achieve a partial rehydration reaction.

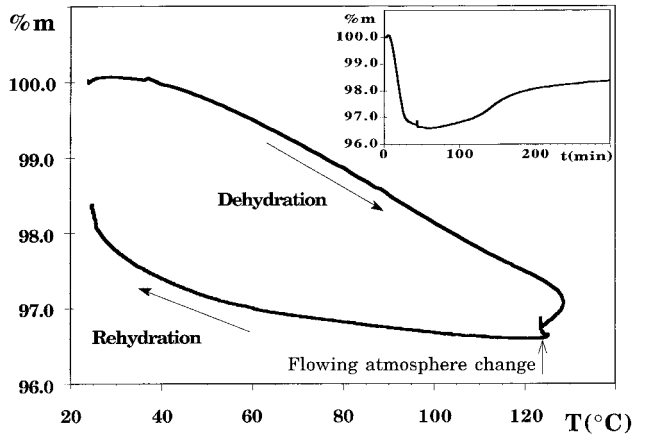

Figure 12. Thermal evolution of compound **2** showing the dehydration and rehydration processes. In the inset we have represented the same data using the time scale in the *x*-axis.

Acknowledgment. We thank very much the Generalitat Valènciana (Grant GV-2227/94) for financial support of this work. M.D.M. thanks the Spanish Ministerio de Educación y Ciencia for a reincorporation contract. The SCSIE of the University of València, Spain, is acknowledged for SEM facilities.

Supporting Information Available: Tables giving crystal data and details of the structure determination, anisotropic thermal parameters, and bond lengths and angles and a figure showing an ORTEP view of the 18.4-Å-type channel (6 pages). Ordering information is given on any current masthead page.

IC960218F